Radio-Frequency Polymer Field-Effect Transistors Characterized by S-Parameters

M. Giorgio and M. Caironi

***Abstract*— Thanks to recent progress in terms of materials properties, polymer field-effect transistors (FETs) operating in the MHz range can be achieved. However, further development toward challenging frequency ranges, for a field accustomed to slow electronic devices, has to be addressed with suitable device design and measurements methodologies. In this letter, we report n-type FETs based on a solution-processed polymer semiconductor where the critical features have been realized by a large-area compatible direct-writing technique, allowing to obtain a maximum frequency of transition of 19 MHz, as measured by means of Scattering Parameters (S-Parameters). This is the first report of solution-processed organic FETs characterized with S-Parameters.**

***Index Terms*— Frequency of transition, high-frequency organic electronics, organic FETs, polymer semiconductors, S-parameters.**

I. Introduction

ORGANIC electronics underwent an impressive development and thanks to its peculiar properties, e.g. high degree of tunability of electronic properties and thin molecular films deposition with scalable processes at low temperature on a wide variety of substrates, represent one of the most promising candidates in the path to ubiquitous, flexible and lightweight low-cost electronics.

To date, organic light emitting diodes (OLEDs) [1] have reached commercial maturity, and significant progress has been achieved for organic solar cells [2], photodetectors [3], biosensors [4] and circuits based on organic transistors [5]. In the case of field effect transistors (FETs), the use of polymer semiconductors has the advantage of achieving superior mechanical properties and easily enabling large-area fabrication techniques, such as printing. Excellent DC performances have been recently achieved owing to an improvement in the understanding of device physics [6], and steady increase in charge carrier mobility [7] and charge carrier injection [8]. Yet, progresses in DC performances are not usually matched by corresponding improvements in AC properties, since typical FET structures devised to test new polymer semiconductors are not optimized for frequency operation. It is instead highly demanded to enhance polymer FET maximum operational frequency, as this would enable a much broader application of this technology. For example, higher operational frequencies are crucial in drivers for high resolution flexible displays [9], radio frequency identification (RFID) systems for smart items identification [10] or wireless communication [11].

A widely adopted figure of merit to assess the maximum operational frequency of transistors is the frequency of transition ($f_T = \frac{g_m}{2\pi C_{TOT}}$, where g_m is the transconductance and C_{TOT} is the total gate capacitance), or unity gain frequency [12], defined as the frequency at which the ratio of the absolute values of the small-signal ac gate current and the small-signal ac drain current equals one. Even if polymer FETs with MHz-range f_T have been achieved, so far their measurement has been complicated by parasitism introduced by the characterization setup itself. In the framework of organic FETs reports, the latter typically becomes dominant already around 1 MHz, and can make the f_T parameter extraction unfeasible already in the tens of MHz range. The reason lies in the commonly adopted characterization techniques that can be referred as *direct measurements*, consisting in directly measuring, typically with low frequency equipment, the AC gate current i_g and the AC drain current i_d as a function of a modulating gate voltage, and then by evaluating the frequency of the crossing point between the two curves. As a consequence, f_T for organic FETs above 10 MHz has been mainly determined so far thanks to an extrapolation from the data obtained at low frequency [13]–[15]. In a single case, for a FET based on evaporated small molecules on electrodes patterned by conventional photolithographic techniques, an f_T of 20 MHz has been measured without extrapolation, thanks to the adoption of inductive probes [16]. For polymer FETs instead, an f_T above 10 MHz was achieved thanks to extrapolation in two cases, in which the device was fabricated by combining direct-writing and printing techniques [17], [18].

Notably, according to recent works, f_T in the GHz range is in principle achievable with organic transistors if a series of requirements are met [19]–[21]. Therefore it is not possible to rely further on direct measurement methods for characterizing the upcoming organic high-frequency devices. For this reason,

Manuscript received March 29, 2019; accepted April 2, 2019. Date of publication April 9, 2019; date of current version May 23, 2019. This work was supported in part by the European Research Council, and in part by the European Union's Horizon 2020 Research and Innovation Programme HEROIC under Grant 638059. The review of this letter was arranged by Editor A. Chin. *(Corresponding author: M. Caironi.)*

M. Giorgio is with the Center for Nano Science and Technology @PoliMi, Istituto Italiano di Tecnologia, 20133 Milan, Italy, and also with the Dipartimento di Elettronica, Informazione e Bioingegneria, Politecnico di Milano, 20133 Milan, Italy.

M. Caironi is with the Center for Nano Science and Technology @PoliMi, Istituto Italiano di Tecnologia, 20133 Milan, Italy (e-mail: mario.caironi@iit.it).

Color versions of one or more of the figures in this letter are available online at http://ieeexplore.ieee.org.

Digital Object Identifier 10.1109/LED.2019.2909844

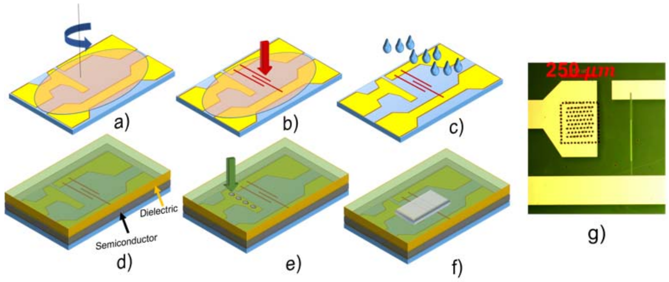

Fig. 1. Sketch of the FETs fabrication process. a) Spin-coating of the nanoparticle ink. b) Laser sintering of source and drain lines. c) Washing off of the unsintered ink d) Deposition of semiconductor and dielectric layers. e) Fabrication of via-holes by laser. f) Inkjet printing of the gate contact. g) Microscope image of the FET prior to gate deposition.

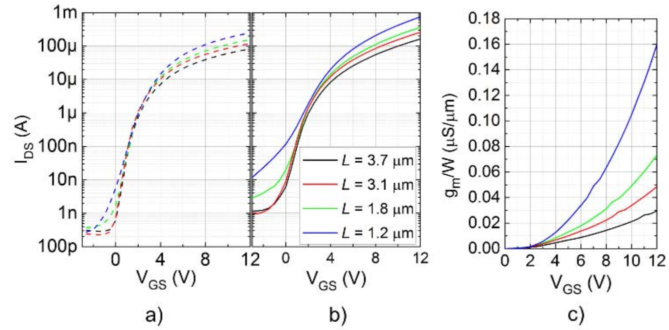

Fig. 2. Transfer characteristics of devices having L ranging from 3.7 μm down to 1.2 μm, W = 1.2 mm, biased a) in linear regime (V_{DS} = 5 V) and b) in saturation regime (V_{DS} = 15 V). c) g_m as a function of V_{GS}, for the different L values, extracted from transfer curves in saturation regime, normalized with respect to W.

two-port Scattering Parameters (S-Parameters) [22], a dimensional quantities which relate the AC currents and voltages between the drain and the gate contacts, become essential also for organic FETs as they readily allow to widen the measurement bandwidth up to the GHz range. Starting from them, a series of parameters can be mathematically computed, such as admittance parameters (Y-Parameters) [22], which are useful to extract physical device parameters, e.g. device capacitances.

Accordingly, organic FETs, which are typically far from being standardized, have to be fabricated compatibly with S-Parameters characterization tools. So far, S-parameters were adopted only by one group for measuring a maximum f_T of 6.7 MHz in organic FETs based on an evaporated small-molecule semiconductor, and realized by using silicon stencil masks to define critical lateral features in the sub-micron range [23]–[25]. At present, no reports describe the use of S-Parameters to measure f_T in the case of FETs based on solution processed organic semiconductors.

In this work, we adopted S-parameters to characterize solution-processed polymer FETs where critical features have been realized by a direct-writing, large-area compatible technique. We fabricated and characterized polymer FETs having channel lengths varying from 3.7 μm down to 1.2 μm and the gate to source and drain overlap lengths ranging from 2.6 μm to 2.3 μm, assessing the scaling of the corresponding f_T at different bias points. For the shortest channel length transistor we obtained a maximum f_T of 19 MHz at the relatively low applied gate-source voltage V_{GS} of 12 V.

II. OFETS FABRICATION PROCESS

A schematic representation of the FET fabrication process flow is illustrated in Figure 1. A 30 nm thick gold pattern, which only serves as interconnection between the probe needles and the actual transistor, was fabricated by standard photolithography on a glass substrate. Then, a polymer transistor was fabricated entirely by means of mask-less processes. In order to achieve high-frequency operation, we adopted a direct-writing method for the definition of the FET critical features. In particular we made use of a femtosecond laser sintering technique for the fabrication of high resolution source and drain metal electrodes, crucial for both the realization of micrometer size channel lengths and the reduction of overlap parasitic capacitances [17]. Such process starts with a uniform deposition of a silver nanoparticle ink film by spin-coating (Fig. 1a). Then, a femtosecond pulsed laser beam (λ = 1030 nm, 67 MHz repetition rate) locally heats the nanoparticle film and patterns the desired geometry of conductive features (Fig. 1b). The unprocessed areas of the film are then washed away using o-xylene, and only the conductive high-resolution patterns are left on the substrate (Fig. 1c).

After the contacts fabrication, the substrate was cleaned by argon plasma and source and drain contacts were modified by growing a 4-(dimethylamino)benzenethiol (DABT) self-assembled monolayer, a process that reduces the contact work function and consequently the energetic barrier for electrons injection into the semiconductor [26]. Afterwards the very well-known semiconducting co-polymer poly[N,N'-bis(2-octyldodecyl)- naphthalene-1,4,5,8-bis(dicarboximide)-2,6-diyl]-alt-5,5′-(2,2′-bithiophene), P(NDI2OD-T2), was deposited by off-center spin-coating in order to achieve uniaxial alignment of polymer backbones, thus improving the charge-carriers transport properties along the alignment direction [27]. Before depositing a 90 nm thick layer of parylene-C, a 20 nm layer of PMMA was deposited by spin-coating to guarantee optimal interfacial properties for an efficient charge transport at the accumulated channel-dielectric interface (Fig. 1d).

To complete the device, via-holes to the gate pad were fabricated by laser ablation (Fig. 1e) and a silver top gate contact was inkjet printed on the channel area using a Fujifilm Dimatix printer and an Ag nanoparticles based ink. The silver layer also connects the gate electrode to the gate interconnection pad (Fig. 1f). Finally, devices were encapsulated by depositing a 500 nm thick parylene capping layer, on top of which a bicomponent epoxy resin (purchased from Robnor Resinlab) was deposited.

III. DC CHARACTERIZATION

We fabricated a set of transistors having channel lengths (L) of 3.7 μm, 3.1 μm, 1.8 μm and 1.2 μm and channel width (W) of 1.2 mm. Transfer curves in the linear and saturation regime of operation are reported in Figure 2a. Devices exhibit good n-type behavior, showing ON/OFF current ratios of at least 5 orders of magnitude despite the short channels. The ON current at $V_{GS} = 12$ V perfectly scales with L in the linear regime of operation ($V_{DS} = 5$ V, Fig. 2a), while the scaling is slightly superlinear in the saturation regime of operation ($V_{DS} = 15$ V, Fig. 2b). This can be also visualized by looking at the channel width normalized transconductance in saturation (g_m/W, Fig. 2c), which increases superlinearly with respect to V_{GS}, reaching at 12 V the value of 0.16 μS/μm for $L = 1.2\ \mu$m and 0.03 μS/μm for $L = 3.7\ \mu$m. The superlinear behavior in saturation becomes more pronounced as the channel length is shortened, as a result of the effect of the higher lateral field on injection and/or transport [28]–[30]. Correspondingly, the apparent mobility (μ_{app}), extracted by computing the derivative of the transfer curve with respect to V_{GS} and assuming the validity of the gradual channel approximation, is substantially constant with respect to L in the linear regime, whilst it increases with decreasing L in the saturation regime. The maximum linear and saturation μ_{app} are 0.35 cm^2/Vs and 1 cm^2/Vs respectively, and are obtained for the shortest channel length transistor ($L = 1.2\ \mu$m). The corresponding effective mobility in saturation, i.e. the apparent mobility corrected by the reliability factor [31], is 0.4 cm^2/Vs.

The output characteristics for longer channel lengths are ideal, while an S-shape at low V_{DS} voltage becomes evident as the channel length is decreased, owing to the presence of a contact resistance effect, estimated to be in the order of 1 kΩcm using the TLM method as a first approximation [32]. The output resistance, extracted by taking the inverse of the slope of the output characteristics at high V_{DS}, ranges from 35 kΩ ($L = 1.2\ \mu$m) to 225 kΩ ($L = 3.7\ \mu$m). The intrinsic gain, calculated by multiplying the output resistance by the transconductance, ranges from 6.65 ($L = 3.7\ \mu$m) to 7.9 ($L = 1.2\ \mu$m).

IV. AC Characterization

f_T is the reference figure of merit that we used to assess the maximum operational frequency of our polymer FETs. In order to derive f_T from S-parameters, the system undergoes first a SOLT (Short-Open-Load-Thru) calibration. By measuring these standards, a 12-terms error correction model [33] is applied to remove non-idealities introduced by the measurement setup itself and to shift the calibration plane at the probe tips.

Then, once the FETs S-Parameters matrix is determined, we compute the hybrid parameter transistor current gain with short-circuited output, $h_{21} = \left.\frac{I_2}{I_1}\right|_{V_2=0}$, where I_2 and I_1 are the drain and gate small-signal currents, respectively, and V_2 is the drain small-signal voltage. To highlight the dependence of h_{21} on physical parameters, its expression can be rewritten by making explicit I_2 and I_1 as $h_{21} = \frac{g_m - j\omega C_{gd}}{j\omega(C_{gs}+C_{gd})}$, where C_{gd} and C_{gs} are the gate-to-drain and the gate-to-source capacitance, respectively. At low frequency h_{21} decreases by 20 dB/decade, while at high frequency it flattens to $C_{gd}/(C_{gs}+C_{gd})$. From its definition, f_T can be identified as the frequency at which h_{21} crosses the 0 dB axis. The measured h_{21} as a function of L is shown in Figure 3a.

For the shortest channel length transistor, h_{21} follows the expected trend and at high frequency, h_{21} flattens at -6 dB, in agreement with the capacitances extracted from the admittance parameters. h_{21} crosses the 0 dB axis at $f_T \approx 19$ MHz. We note the effect of the interconnections series and parallel parasitic impedances, quantified through a two-step de-embedding procedure [34], are negligible in our conditions and for the frequency range of interest.

Such a high f_T is achieved at a relatively low voltage ($V_{GS} = 12$ V). As a result, this is the fastest organic transistor measured with S-parameters and in general one of the fastest organic transistors if we look at the frequency of transition normalized for the applied gate-source voltage,

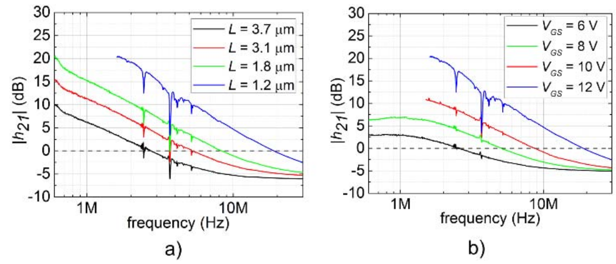

Fig. 3. a) Bode plot of $|h_{21}|$ highlighting the transition frequency dependence on a) transistor channel length (with $V_{GS} = 12$ V and $V_{DS} = 15$ V) and b) bias point of operation for the shortest channel length transistor ($L = 1.2\ \mu$m, $V_{DS} = 6$, 8 ,10, 15 V). Spurious interferences, originated from the DC voltage source adopted, are visible from 2 to 5 MHz.

TABLE I

Summary of Transistors g_m and C_{TOT} for Different L ($V_{GS} = 12$ V and $V_{DS} = 15$ V) and Comparison Between Measured f_T and Computed f_T

Channel length	g_m	C_{TOT}	L_{ov}	Calculated f_T	Measured f_T
L = 1.2 μm	190 μS	1.27 pF	2.3 μm	24 MHz	19 MHz
L = 1.8 μm	90 μS	1.4 pF	2.6 μm	10 MHz	8.3 MHz
L = 3.1 μm	60 μS	1.47 pF	2.5 μm	6.5 MHz	5.2 MHz
L = 3.7 μm	35 μS	1.46 pF	2.6 μm	3.8 MHz	2.8 MHz

f_T/V_{GS} [18], here reaching 1.6 MHz/V. The measured g_m, C_{TOT}, gate to source and drain geometric overlap length (L_{ov}) and f_T are reported in Table 1 together with f_T expected from first principle calculations, where g_m is extracted from quasi-static transfer curves in Figure 2b, and C_{TOT} is extracted from Y-parameters, being $|Y_{11}| = \omega C_{TOT}$. Also C_{gd} can be extracted from Y-parameters according to $|Y_{12}| = \omega C_{gd}$, finally obtaining also C_{gs} as $C_{gs} = C_{TOT} - C_{gd}$.

In the case of the shortest channel length transistor ($L = 1.2\ \mu$m), we also characterized the dependence of the h_{21} parameter on the FET voltage bias point in saturation, by applying $V_{GS} = 6$, 8, 10, 12 V and $V_{DS} = 6$, 8, 10, 15 V, respectively (Fig. 3b). As a result, f_T increases from 2.5 MHz at $V_{GS} = V_{DS} = 6$ V to 19 MHz at $V_{GS} = 12$ V and $V_{DS} = 15$ V. We successfully checked that measured f_T values are consistent with predicted values also in this case by extracting g_m from the static curves and C_{TOT}, constant with bias at 1.27 pF, from the Y-parameters.

V. Conclusions

For the first time for solution-processed polymer field-effect transistors, we resorted to S-Parameters for reliable determination of the frequency of transition without extrapolations, characterizing devices reaching $f_T = 19$ MHz at 12 V. As further optimization of architectures and reduction of contact resistance, in combination with higher mobility polymers, should allow achieving the hundreds of MHz range, it will be necessary to adopt S-Parameters measurements for the future development of high-frequency polymer electronics.

Acknowledgement

The authors gratefully acknowledge A. Perinot for helping with the design of the devices and their fabrication, and M. Butti and L. Criante for their support with laser sintering. This work has been partially carried out at Polifab, the micro- and nano-technology center of the Politecnico di Milano.

References

[1] B. Geffroy, P. Le Roy, and C. Prat, "Organic light-emitting diode (OLED) technology: Materials, devices and display technologies," *Polymer Int.*, vol. 55, no. 6, pp. 572–582, Jun. 2006. doi: 10.1002/pi.1974.

[2] O. Inganäs, "Organic photovoltaics over three decades," *Adv. Mater.*, vol. 30, no. 35, Aug. 2018, Art. no. 1800388. doi: 10.1002/adma.201800388.

[3] K. J. Baeg, M. Binda, D. Natali, M. Caironi, and Y. Y. Noh, "Organic light detectors: Photodiodes and phototransistors," *Adv. Mater.*, vol. 25, no. 31, pp. 4267–4295, Aug. 2013. doi: 10.1002/adma.201204979.

[4] L. Torsi, M. Magliulo, K. Manoli, and G. Palazzo, "Organic field-effect transistor sensors: A tutorial review," *Chem. Soc. Rev.*, vol. 42, no. 22, pp. 8612–8628, 2013. doi: 10.1039/C3CS60127G.

[5] J. S. Chang, A. F. Facchetti, and R. Reuss, "A circuits and systems perspective of organic/printed electronics: Review, challenges, and contemporary and emerging design approaches," *IEEE J. Emerg. Sel. Topics Circuits Syst.*, vol. 7, no. 1, pp. 7–26, Mar. 2017. doi: 10.1109/JETCAS.2017.2673863.

[6] H. Sirringhaus, "Device physics of solution-processed organic field-effect transistors," *Adv. Mater.*, vol. 17, no. 20, pp. 2411–2425, Oct. 2005. doi: 10.1002/adma.200501152.

[7] A. F. Paterson, S. Singh, K. J. Fallon, T. Hodsden, Y. Han, B. C. Schroeder, H. Bronstein, M. Heeney, I. McCulloch, and T. D. Anthopoulos, "Recent progress in high-mobility organic transistors: A reality check," *Adv. Mater.*, vol. 30, no. 36, Sep. 2018, Art. no. 1801079. doi: 10.1002/adma.201801079.

[8] D. Natali and M. Caironi, "Charge injection in solution-processed organic field-effect transistors: Physics, models and characterization methods," *Adv. Mater.*, vol. 24, no. 11, pp. 1357–1387, Mar. 2012. doi: 10.1002/adma.201104206.

[9] P. Heremans, "Electronics on plastic foil, for applications in flexible OLED displays, sensor arrays and circuits," in *Proc. 21st Int. Workshop Act.-Matrix Flatpanel Displays Devices*, Jul. 2014, pp. 1–4. doi: 10.1109/AM-FPD.2014.6867106.

[10] E. Cantatore, T. C. T. Geuns, G. H. Gelinck, E. van Veenendaal, A. F. Gruijthuijsen, L. Schrijnemakers, S. Drews, and D. M. de Leeuw, "A 13.56-MHz RFID system based on organic transponders," *IEEE J. Solid-State Circuits*, vol. 42, no. 1, pp. 84–92, Jan. 2007. doi: 10.1109/JSSC.2006.886556.

[11] A. Facchetti, "Printed diodes operating at mobile phone frequencies," *Proc. Nat. Acad. Sci. USA*, vol. 111, no. 33, pp. 11917–11918, Aug. 2014. doi: 10.1073/pnas.1412312111.

[12] H. Klauk, "Organic thin film transistors," *Chem. Soc. Rev.*, vol. 39, no. 7, pp. 2643–2666, Apr. 2010. doi: 10.1039/B909902F.

[13] K. Nakayama, M. Uno, T. Uemura, N. Namba, Y. Kanaoka, T. Kato, M. Katayama, C. Mitsui, T. Okamoto, and J. Takeya, "High-mobility organic transistors with wet-etch-patterned top electrodes: A novel patterning method for fine-pitch integration of organic devices," *Adv. Mater. Interfaces*, vol. 1, no. 5, Apr. 2014, Art. no. 1300124. doi: 10.1002/admi.201300124.

[14] M. Kitamura and Y. Arakawa, "High current-gain cutoff frequencies above 10 MHz in n-channel C_{60} and p-channel pentacene thin-film transistors," *Jpn. J. Appl. Phys.*, vol. 50, no. 1S2, Jan. 2011, Art. no. 01BC01. doi: 10.1143/JJAP.50.01BC01.

[15] T. Uemura, T. Matsumoto, K. Miyake, M. Uno, S. Ohnishi, T. Kato, M. Katayama, S. Shinamura, M. Hamada, M.-J. Kang, K. Takimiya, C. Mitsui, T. Okamoto, and J. Takeya, "Split-gate organic field-effect transistors for high-speed operation," *Adv. Mater.*, vol. 26, no. 19, pp. 2983–2988, May 2014. doi: 10.1002/adma.201304976.

[16] M. Uno, B.-S. Cha, Y. Kanaoka, and J. Takeya, "High-speed organic transistors with three-dimensional organic channels and organic rectifiers based on them operating above 20 MHz," *Organic Electron.*, vol. 20, pp. 119–124, May 2015. doi: 10.1016/j.orgel.2015.02.005.

[17] A. Perinot, P. Kshirsagar, M. A. Malvindi, P. P. Pompa, R. Fiammengo, and M. Caironi, "Direct-written polymer field-effect transistors operating at 20 MHz," *Sci. Rep.*, vol. 6, Dec. 2016, Art. no. 38941. doi: 10.1038/srep38941.

[18] A. Perinot and M. Caironi, "Accessing MHz operation at 2 V with field-effect transistors based on printed polymers on plastic," *Adv. Sci.*, vol. 6, no. 4, Dec. 2018, Art. no. 1801566. doi: 10.1002/advs.201801566.

[19] H. Klauk, "Will we see gigahertz organic transistors?" *Adv. Electron. Mater.*, vol. 4, no. 10, Oct. 2018, Art. no. 1700474. doi: 10.1002/aelm.201700474.

[20] M. Caironi, E. Gili, and H. Sirringhaus, "Ink-jet printing of downscaled organic electronic devices," in *Organic Electronics II: More Materials and Applications*. Weinheim, Germany: Whiley-VCH, 2012, pp. 281–326.

[21] A. Perinot, M. Giorgio, and M. Caironi, "Development of organic field-effect transistors for operation at high frequency," in *Flexible Carbon-based Electronics*. Weinheim, Germany: Whiley-VCH, 2018, pp. 71–94.

[22] Agilent Technologies, "S-parameter design," Agilent Technol., Santa Clara, CA, USA, Appl. Note 154, 2006.

[23] T. Zaki, R. Rödel, F. Letzkus, H. Richter, U. Zschieschang, H. Klauk, and J. N. Burghartz, "S-parameter characterization of submicrometer low-voltage organic thin-film transistors," *IEEE Electron Device Lett.*, vol. 34, no. 4, pp. 520–522, Apr. 2013. doi: 10.1109/LED.2013.2246759.

[24] T. Zaki, R. Rödel, F. Letzkus, H. Richter, U. Zschieschang, H. Klauk, and J. N. Burghartz, "AC characterization of organic thin-film transistors with asymmetric gate-to-source and gate-to-drain overlaps," *Organic Electron.*, vol. 14, no. 5, pp. 1318–1322, 2013. doi: 10.1016/J.ORGEL.2013.02.014.

[25] J. W. Borchert, U. Zschieschang, F. Letzkus, M. Giorgio, M. Caironi, J. N. Burghartz, S. Ludwigs, and H. Klauk, "Record static and dynamic performance of flexible organic thin-film transistors," in *IEDM Tech. Dig.*, Dec. 2018, pp. 1–38. doi: 10.1109/IEDM.2018.8614641.

[26] M. Kitamura, Y. Kuzumoto, S. Aomori, M. Kamura, J. H. Na, and Y. Arakawa, "Threshold voltage control of bottom-contact *n*-channel organic thin-film transistors using modified drain/source electrodes," *Appl. Phys. Lett.*, vol. 94, no. 8, p. 65, Feb. 2009. doi: 10.1063/1.3090489.

[27] S. G. Bucella, A. Luzio, E. Gann, L. Thomsen, C. R. McNeill, G. Pace, A. Perinot, Z. Chen, A. Facchetti, and M. Caironi, "Macroscopic and high-throughput printing of aligned nanostructured polymer semiconductors for MHz large-area electronics," *Nature Commun.*, vol. 6, p. 8394, Sep. 2015. doi: 10.1038/ncomms9394.

[28] A. Luzio, L. Criante, V. D'Innocenzo, and M. Caironi, "Control of charge transport in a semiconducting copolymer by solvent-induced long-range order," *Sci. Rep.*, vol. 3, Dec. 2013, Art. no. 3425. doi: 10.1038/srep03425.

[29] D. Fazzi and M. Caironi, "Multi-length-scale relationships between the polymer molecular structure and charge transport: The case of poly-naphthalene diimide bithiophene," *Phys. Chem. Chem. Phys.*, vol. 17, no. 14, pp. 8573–8590, Feb. 2015. doi: 10.1039/C5CP00523J.

[30] L. Wang, D. Fine, D. Basu, and A. Dodabalapur, "Electric-field-dependent charge transport in organic thin-film transistors," *J. Appl. Phys.*, vol. 101, no. 5, Mar. 2007, Art. no. 054515. doi: 10.1063/1.2496316.

[31] H. H. Choi, K. Cho, C. D. Frisbie, H. Sirringhaus, and V. Podzorov, "Critical assessment of charge mobility extraction in FETs," *Nature Mater.*, vol. 17, no. 1, p. 2, Dec. 2017. doi: 10.1038/nmat5035.

[32] Y. Xu, R. Gwoziecki, I. Chartier, R. Coppard, F. Balestra, and G. Ghibaudo, "Modified transmission-line method for contact resistance extraction in organic field-effect transistors," *Appl. Phys. Lett.*, vol. 97, no. 6, p. 171, Aug. 2010. doi: 10.1063/1.3479476.

[33] Agilent Technologies, "Applying error correction to network analyzer measurements," Santa Clara, CA, USA, Agilent Technol., Appl. Note 1287-3.

[34] M. C. A. M. Koolen, J. A. M. Geelen, and M. P. J. G. Versleijen, "An improved de-embedding technique for on-wafer high-frequency characterization," in *Proc. Bipolar Circuits Technol. Meeting*, Sep. 1991, pp. 188–191. doi: 10.1109/BIPOL.1991.160985.